European Journal of Inorganic Chemistry

Supporting Information

Spin Crossover and Field-Induced Single-Molecule Magnet Behaviour in Co(II) Complexes Based on Terpyridine with Tetrathiafulvalene Analogues

Siham Tiaouinine, Jessica Flores Gonzalez, Bertrand Lefeuvre, Thierry Guizouarn, Marie Cordier, Vincent Dorcet, Lakehmici Kaboub, Olivier Cador, and Fabrice Pointillart*

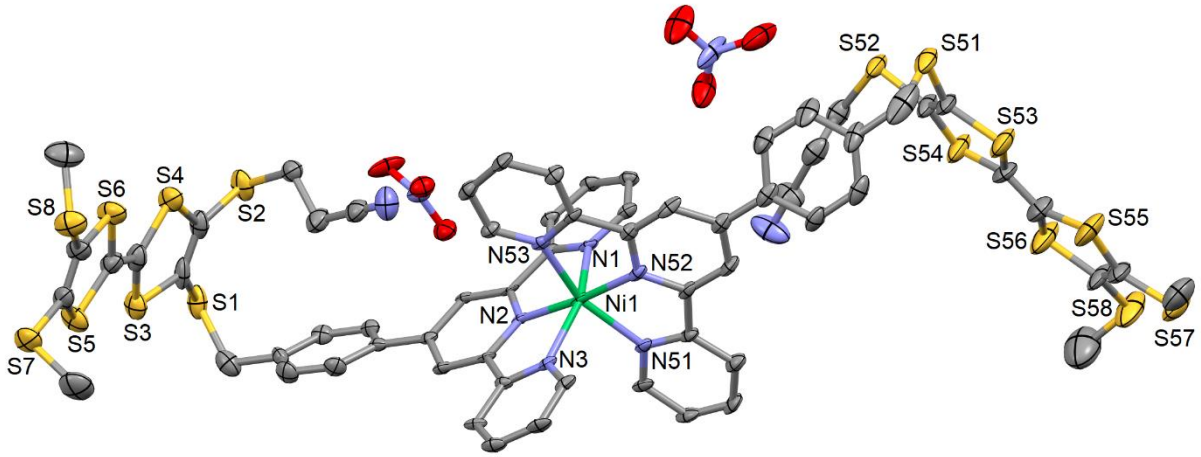

Figure S1. ORTEP view of the asymmetric unit for **1**. Thermal ellipsoids are drawn at 30% probability. Hydrogen atoms are omitted for clarity.

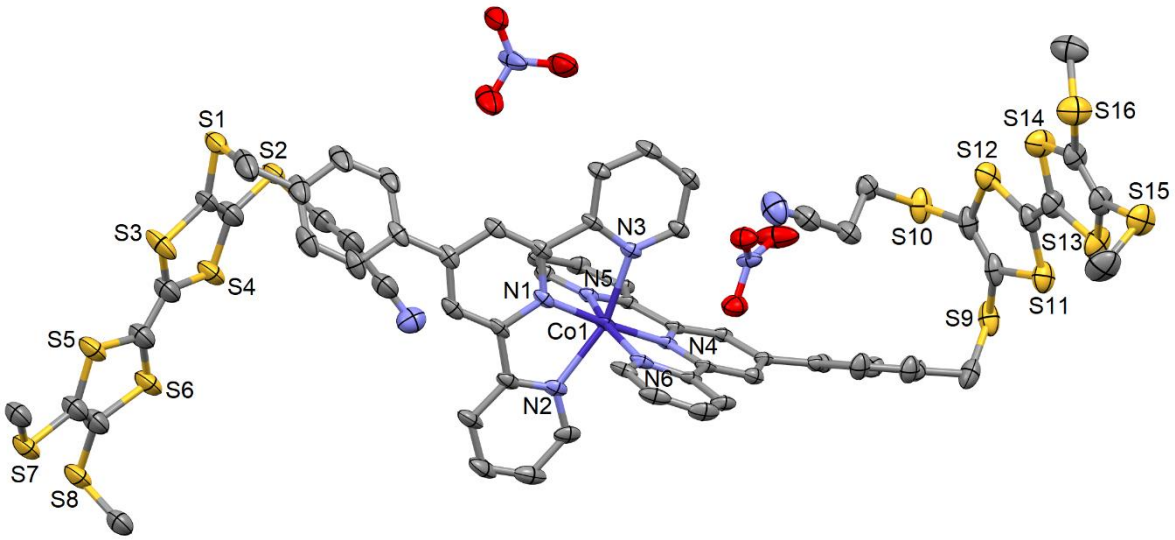

Figure S2. ORTEP view of the asymmetric unit for **2**. Thermal ellipsoids are drawn at 30% probability. Hydrogen atoms are omitted for clarity.

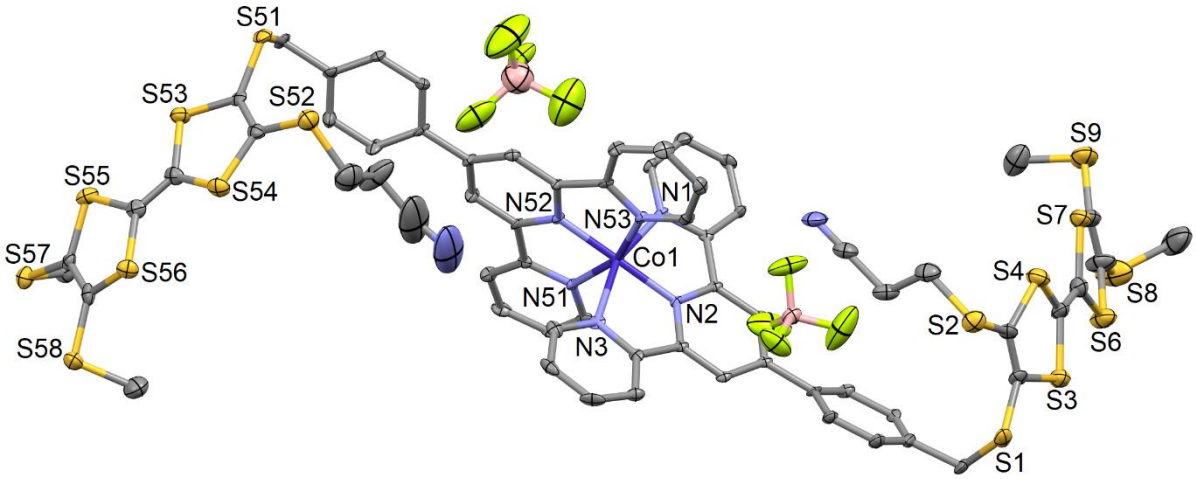

Figure S3. ORTEP view of the asymmetric unit for **3**. Thermal ellipsoids are drawn at 30% probability. Hydrogen atoms are omitted for clarity.

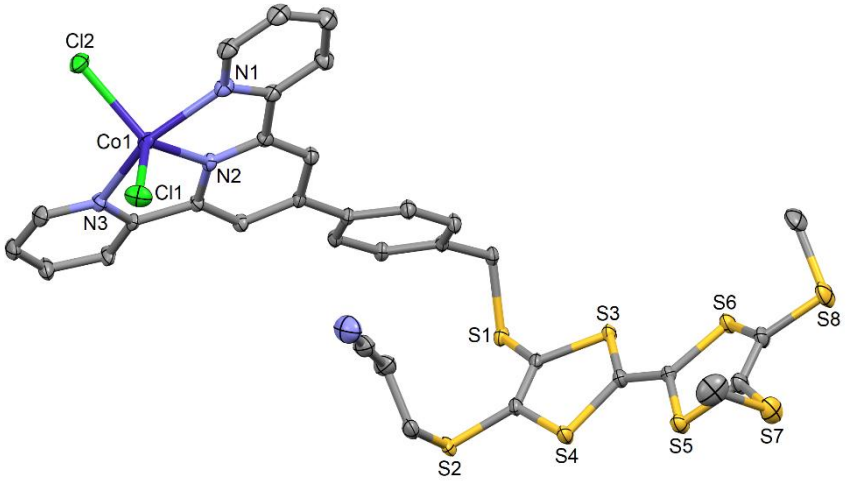

Figure S4. ORTEP view of the asymmetric unit for **4**. Thermal ellipsoids are drawn at 30% probability. Hydrogen atoms and N,N-Dimethylformamide molecule of crystallization are omitted for clarity.

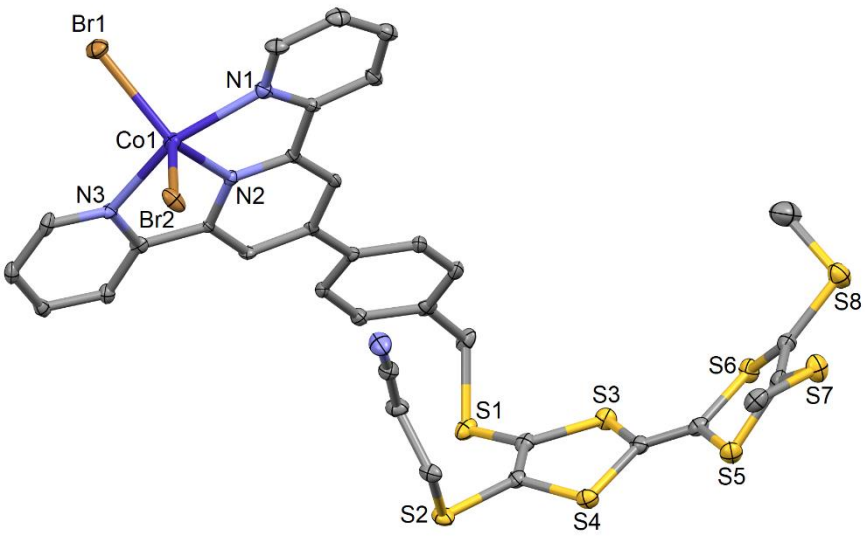

Figure S5. ORTEP view of the asymmetric unit for **5**. Thermal ellipsoids are drawn at 30% probability. Hydrogen atoms and N,N-Dimethylformamide molecule of crystallization are omitted for clarity.

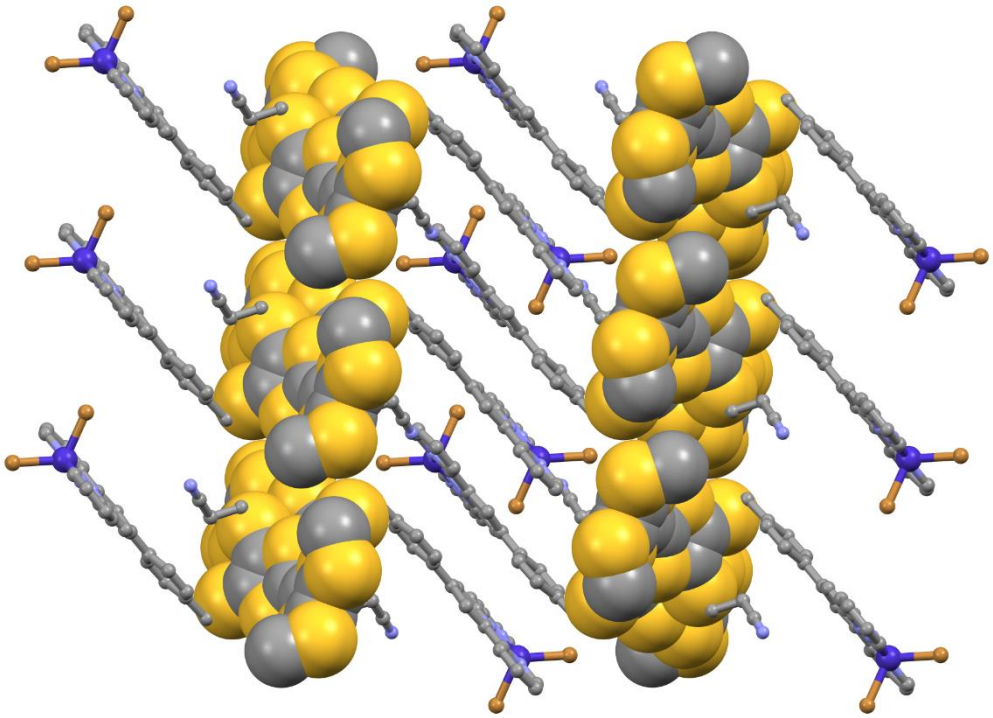

Figure S6. Crystal packing of **5**. The DMT-TTF fragment is drawn in space fill representation to highlight the 1D S···S contacts.

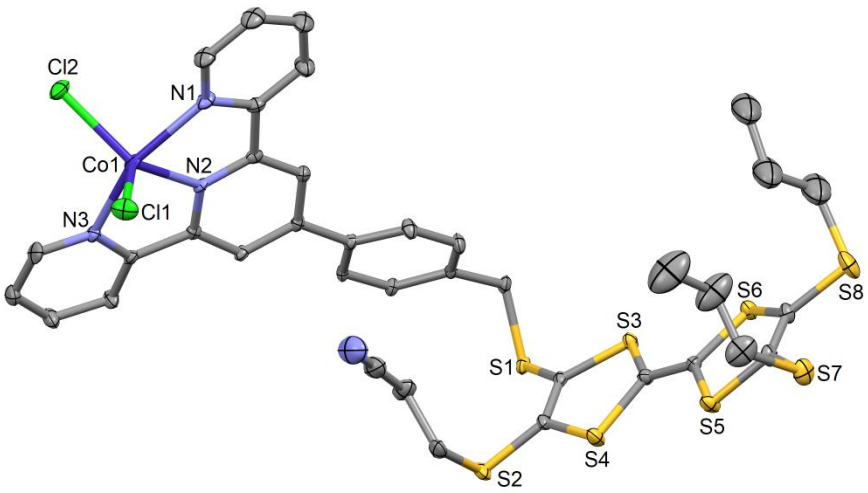

Figure S7. ORTEP view of the asymmetric unit for **6**. Thermal ellipsoids are drawn at 30% probability. Hydrogen atoms, N,N-Dimethylformamide and diethylether molecules of crystallization are omitted for clarity.

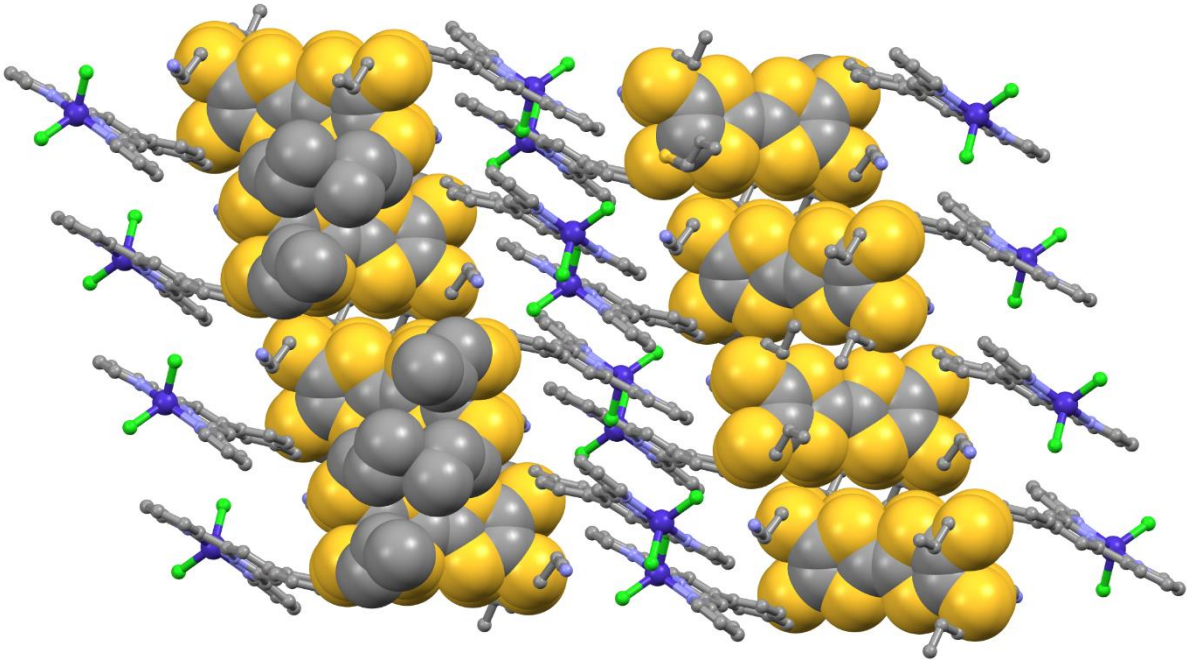

Figure S8. Crystal packing of **6**. The DMT-TTF fragment is drawn in space fill representation to highlight the 1D S···S contacts.

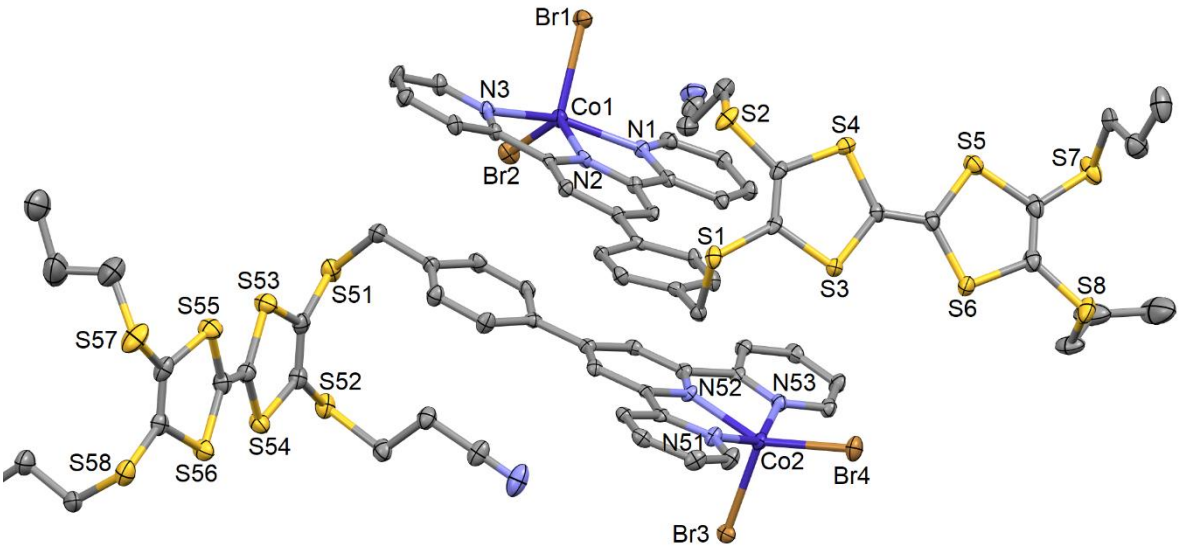

Figure S9. ORTEP view of the asymmetric unit for **7**. Thermal ellipsoids are drawn at 30% probability. Hydrogen atoms, N,N-Dimethylformamide molecules of crystallization are omitted for clarity.

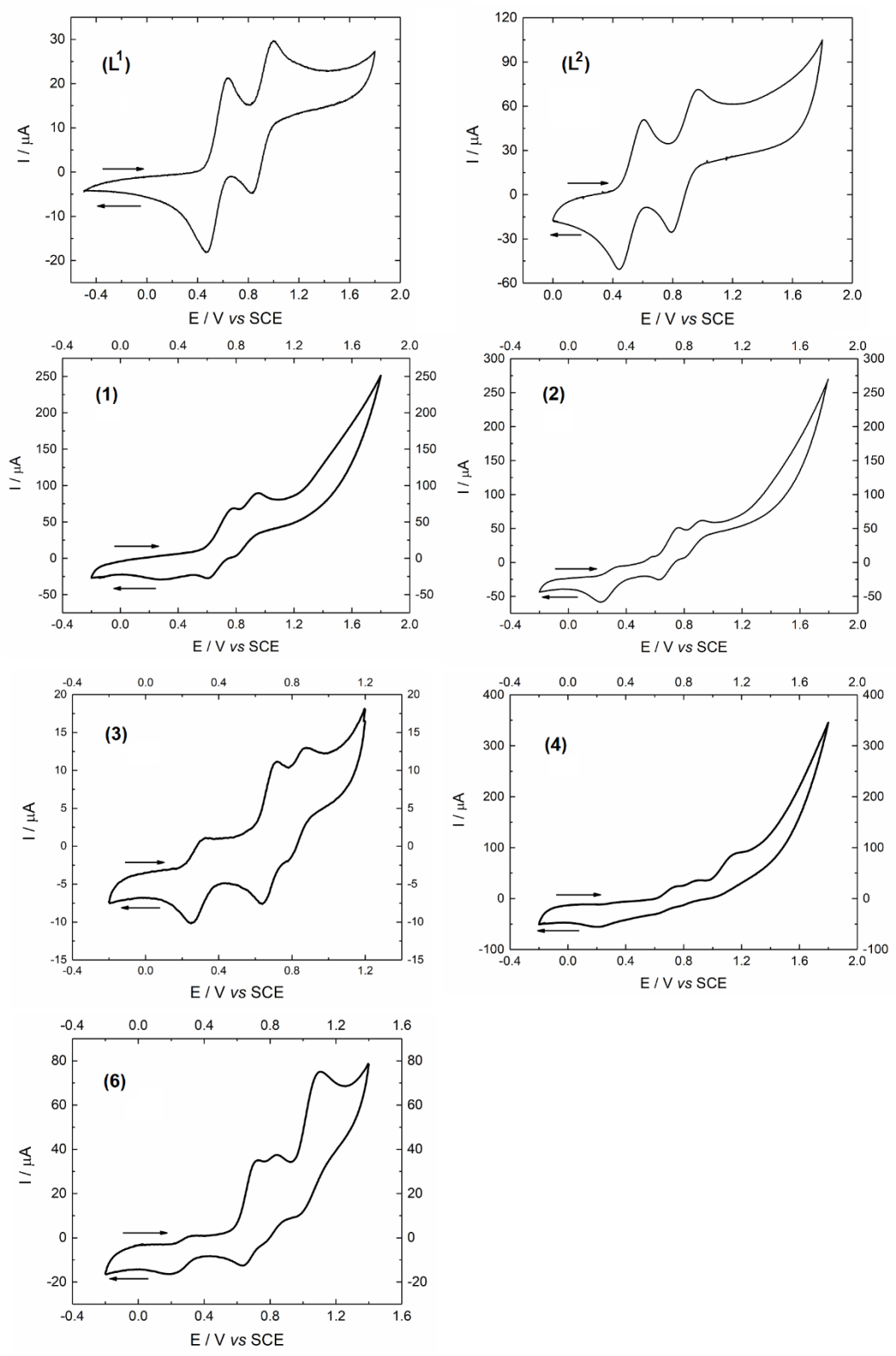

Figure S10. Cyclic voltammograms of the ligands $\mathbf{L^1}$ and $\mathbf{L^2}$ in CH_2Cl_2, and complexes **1-4** and **6** in DMF at a scan rate of 100 $mV \cdot s^{-1}$. The potentials were measured *vs*. a saturated calomel electrode (SCE) with Pt wires as working and counter electrodes.

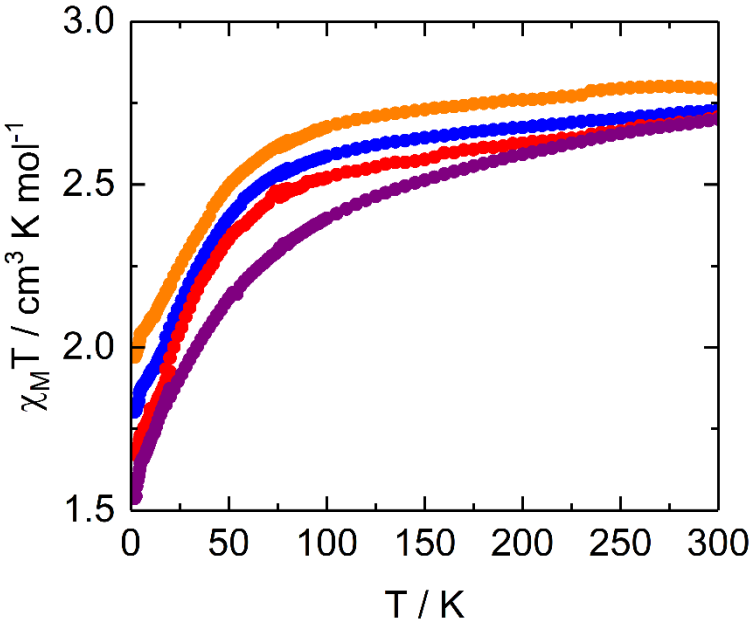

Figure S11. Thermal dependence of the $\chi_M T$ product between 2 and 300 K for **4** (blue spots), **5** (red spots), **6** (orange spots) and **7** (purple spots).

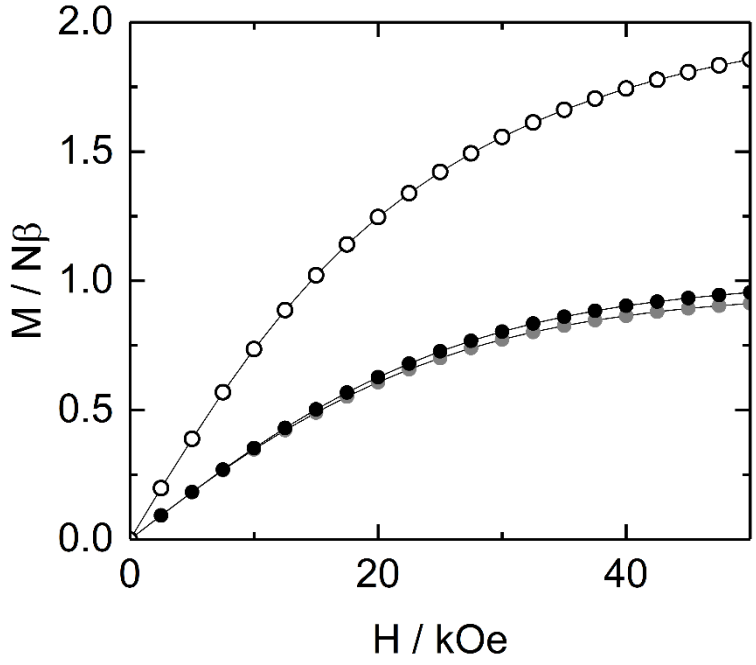

Figure S12. Field dependence of the magnetization at 2 K for **1** (open black circles), **2** (full black circles) and **3** (full gray circles).

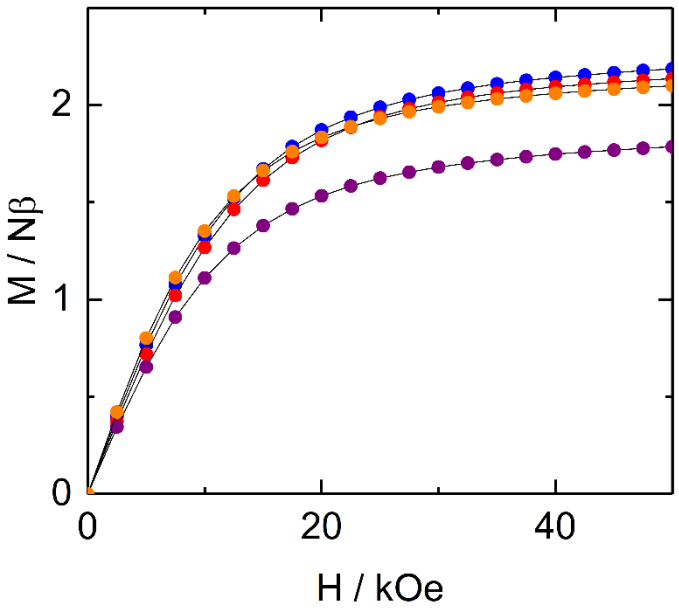

Figure S13. Field dependence of the magnetization at 2 K for **4** (blue spots), **5** (red spots), **6** (orange spots) and **7** (purple spots).

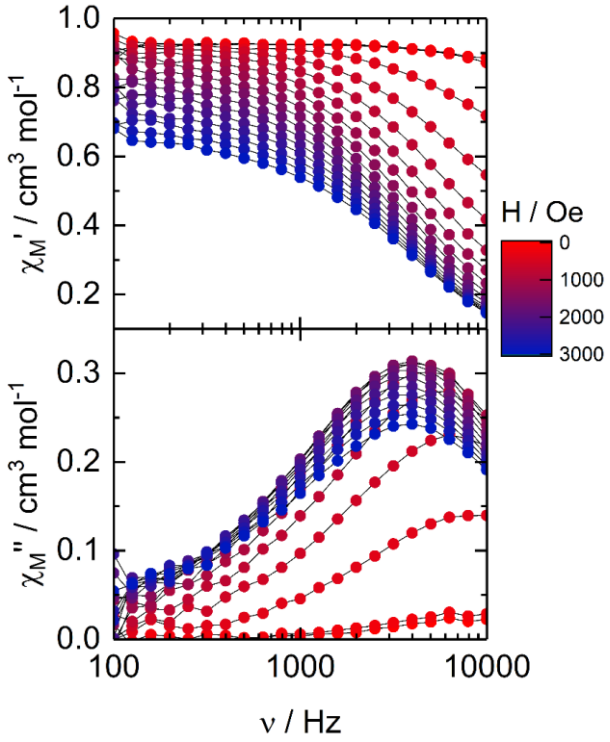

Figure S14. In-phase (top) and out-of-phase (bottom) components of the ac magnetic susceptibility for **4** at 2 K under a DC magnetic field from 0 to 3000 Oe.

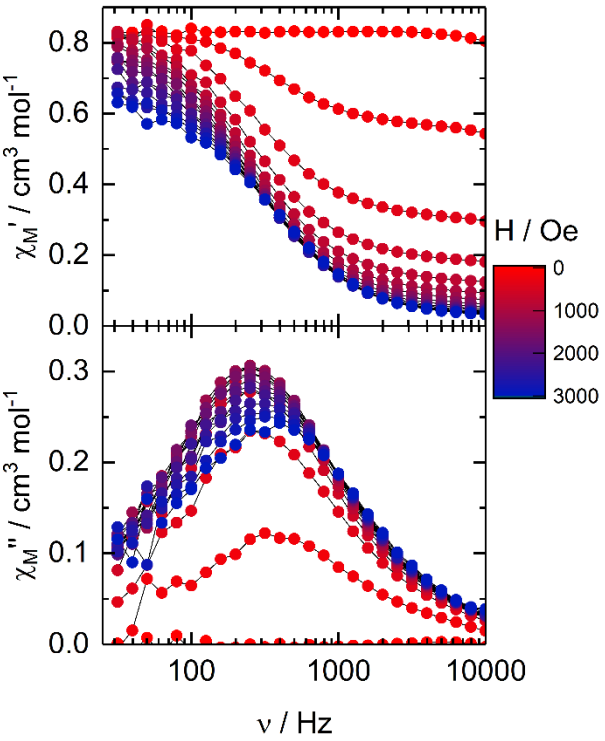

Figure S15. In-phase (top) and out-of-phase (bottom) components of the ac magnetic susceptibility for **5** at 2 K under a DC magnetic field from 0 to 3000 Oe.

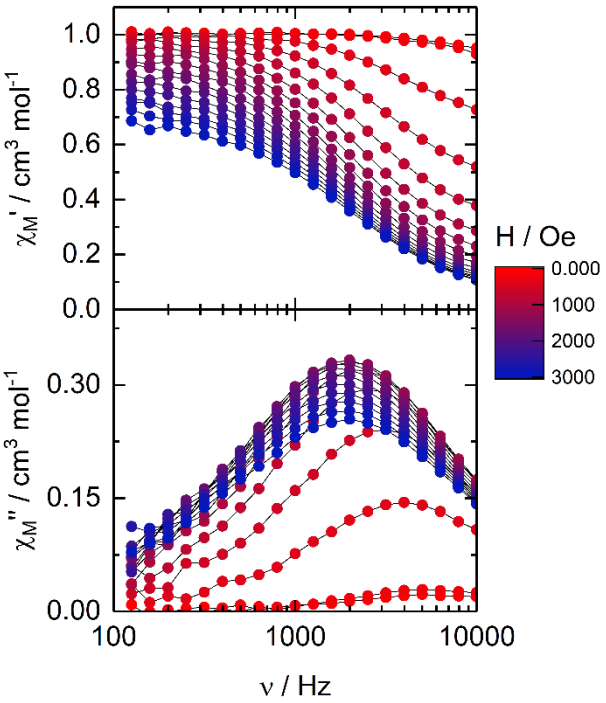

Figure S16. In-phase (top) and out-of-phase (bottom) components of the ac magnetic susceptibility for **6** at 2 K under a DC magnetic field from 0 to 3000 Oe.

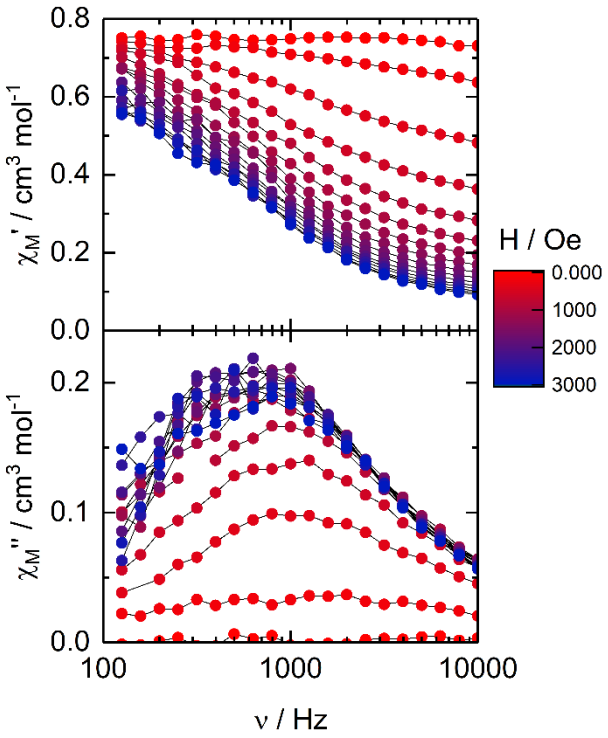

Figure S17. In-phase (top) and out-of-phase (bottom) components of the ac magnetic susceptibility for **7** at 2 K under a DC magnetic field from 0 to 3000 Oe.

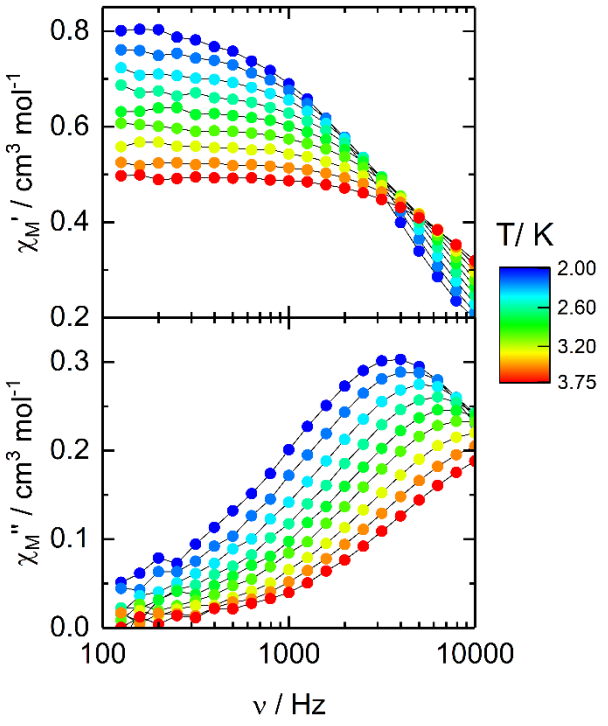

Figure S18. Frequency dependence of the in-phase (top) and out-of-phase (bottom) component of the magnetic susceptibility under an applied magnetic field of 1700 Oe between 2 and 3.75 K for **4**.

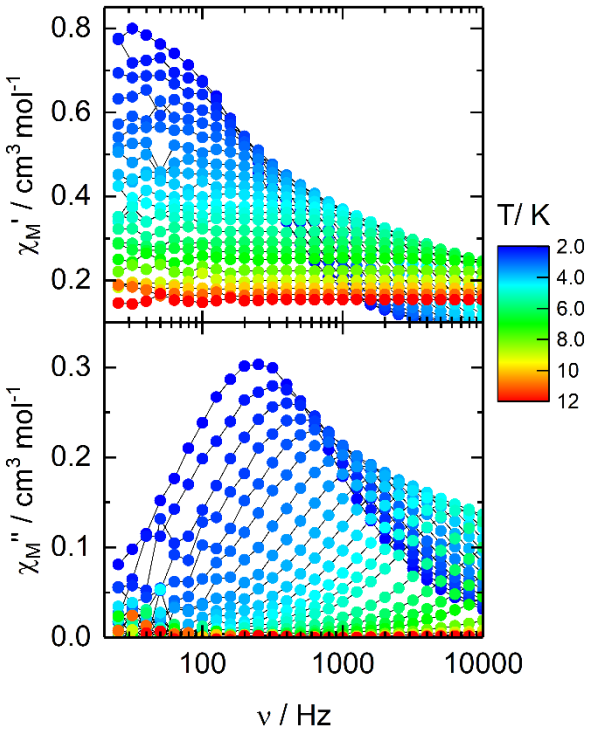

Figure S19. Frequency dependence of the in-phase (top) and out-of-phase (bottom) component of the magnetic susceptibility under an applied magnetic field of 1000 Oe between 2 and 12 K for **5**.

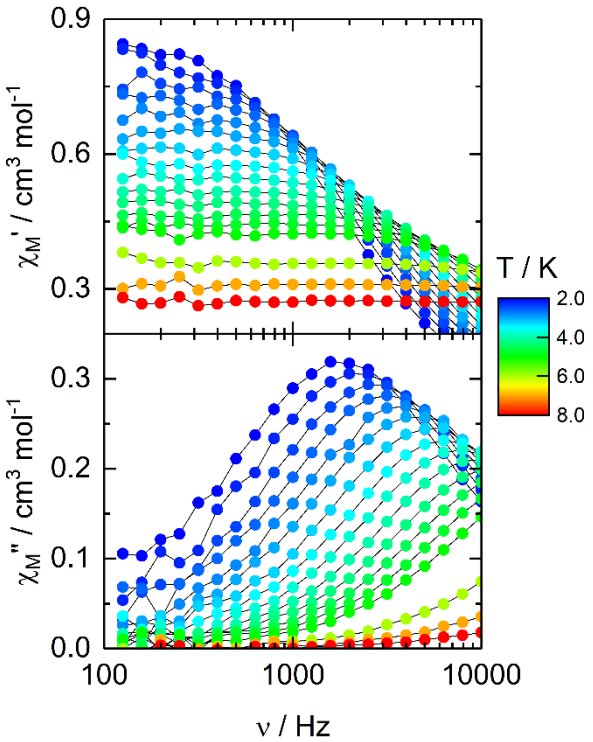

Figure S20. Frequency dependence of the in-phase (top) and out-of-phase (bottom) component of the magnetic susceptibility under an applied magnetic field of 2000 Oe between 2 and 8 K for **6**.

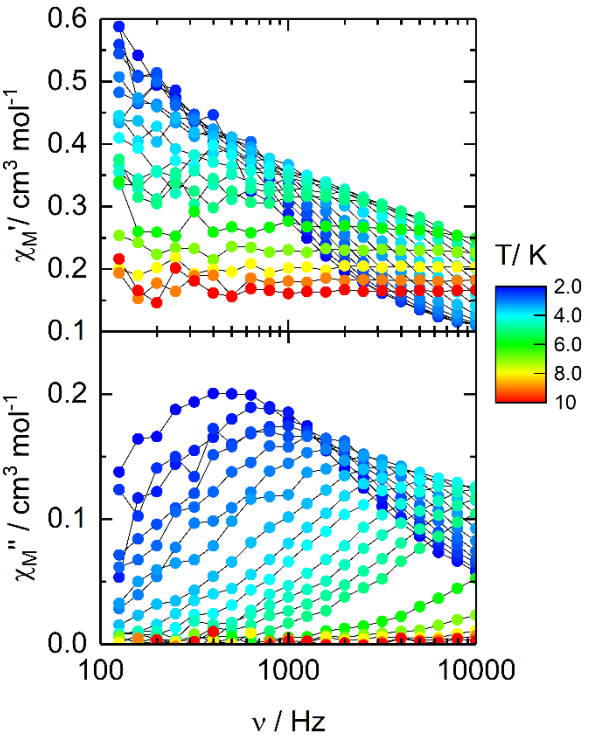

Figure S21. Frequency dependence of the in-phase (top) and out-of-phase (bottom) component of the magnetic susceptibility under an applied magnetic field of 2200 Oe between 2 and 10 K for **7**.

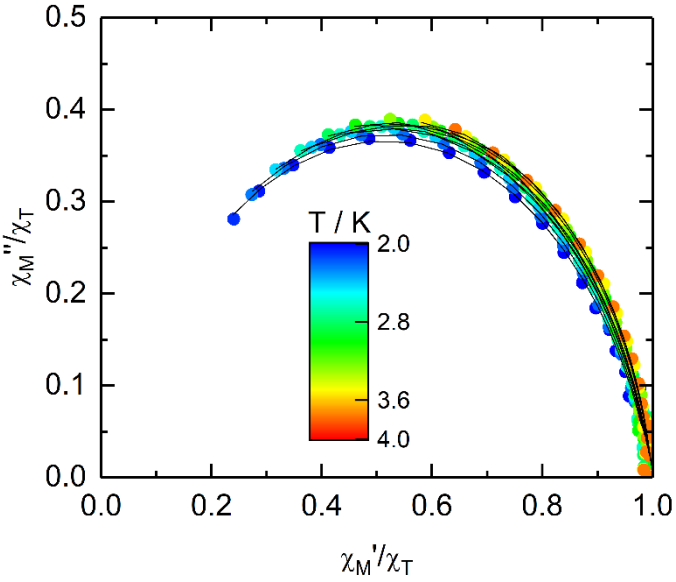

Figure S22. Normalized Cole-Cole plot for **4** at several temperatures between 2 and 4 K under an applied magnetic field of 1700 Oe. Black lines are the best fitted curves.

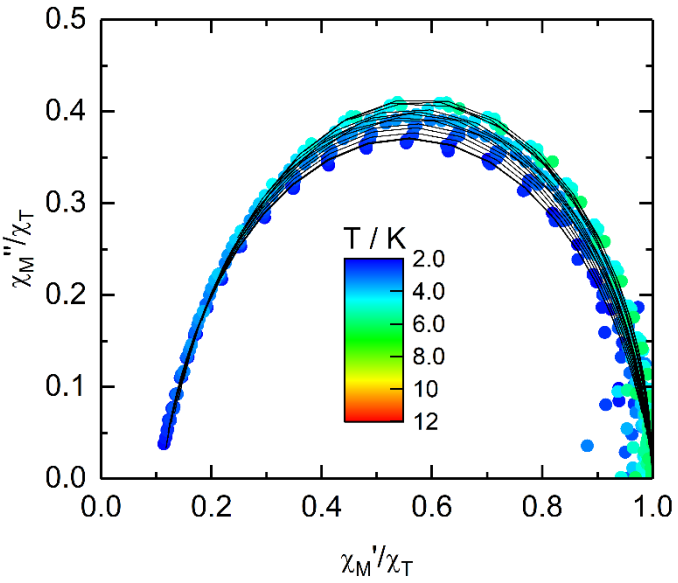

Figure S23. Normalized Cole-Cole plot for **5** at several temperatures between 2 and 12 K under an applied magnetic field of 1000 Oe. Black lines are the best fitted curves.

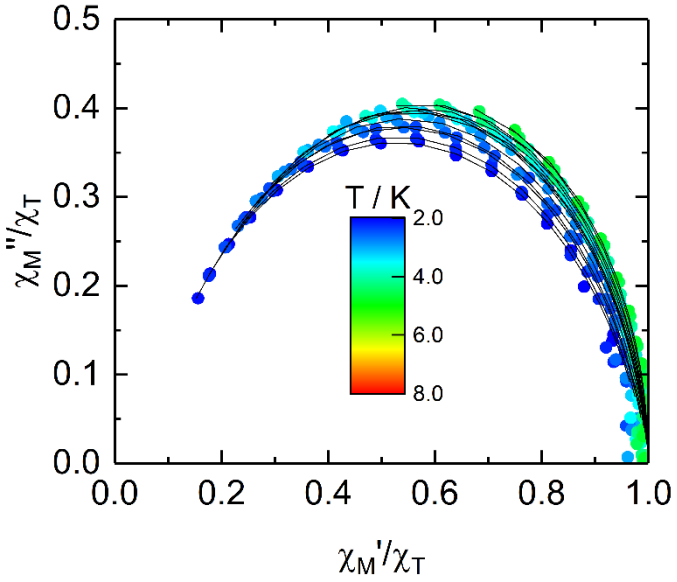

Figure S24. Normalized Cole-Cole plot for **6** at several temperatures between 2 and 8 K under an applied magnetic field of 2000 Oe. Black lines are the best fitted curves.

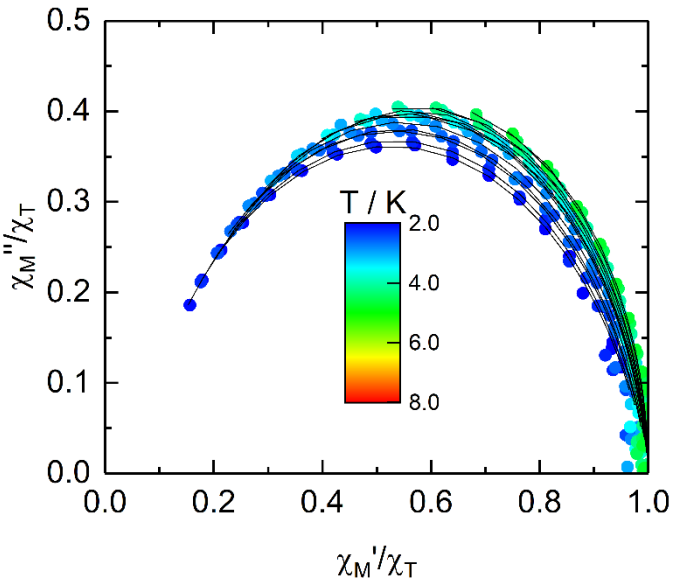

Figure S25. Normalized Cole-Cole plot for **7** at several temperatures between 2 and 8 K under an applied magnetic field of 2200 Oe. Black lines are the best fitted curves.

Extended Debye model.

$$\chi_M' = \chi_S + (\chi_T - \chi_S)\frac{1+(\omega\tau)^{1-\alpha}\sin\left(\alpha\frac{\pi}{2}\right)}{1+2(\omega\tau)^{1-\alpha}\sin\left(\alpha\frac{\pi}{2}\right)+(\omega\tau)^{2-2\alpha}}$$

$$\chi_M'' = (\chi_T - \chi_S)\frac{(\omega\tau)^{1-\alpha}\cos\left(\alpha\frac{\pi}{2}\right)}{1+2(\omega\tau)^{1-\alpha}\sin\left(\alpha\frac{\pi}{2}\right)+(\omega\tau)^{2-2\alpha}}$$

With χ_T the isothermal susceptibility, χ_S the adiabatic susceptibility, τ the relaxation time and α an empiric parameter which describe the distribution of the relaxation time. For SMM with only one relaxing object α is close to zero. The extended Debye model was applied to fit simultaneously the experimental variations of χ_M' and χ_M'' with the frequency ν of the oscillating field ($\omega = 2\pi\nu$). Typically, only the temperatures for which a maximum on the χ'' vs. f curves, have been considered. The best fitted parameters τ, α, χ_T, χ_S are listed in Tables S3-S10 with the coefficient of determination R^2.

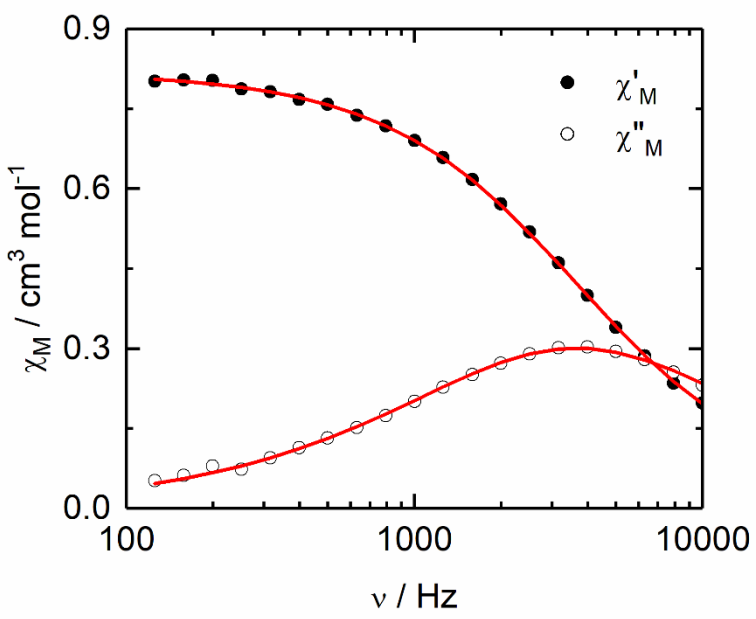

Figure S26. Frequency dependence of the in-phase (χ_M') and out-of-phase (χ_M") components of the ac susceptibility measured on powder at 2 K and 1700 Oe with the best fitted curves (red lines) for **4**.

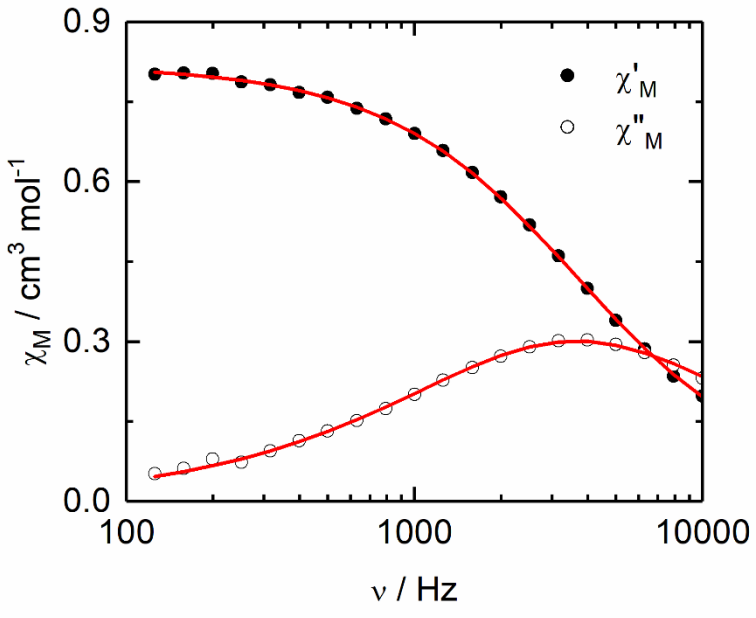

Figure S27. Frequency dependence of the in-phase (χ_M') and out-of-phase (χ_M") components of the ac susceptibility measured on powder at 2 K and 1000 Oe with the best fitted curves (red lines) for **5**.

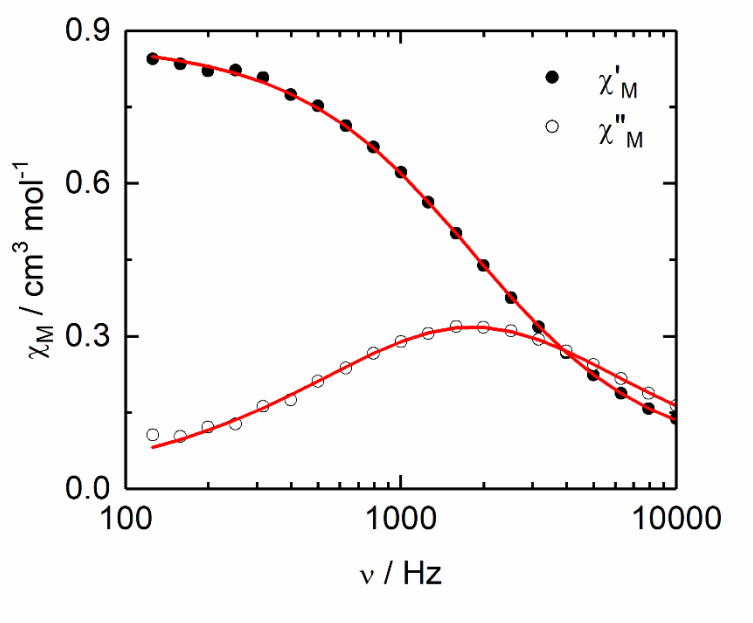

Figure S28. Frequency dependence of the in-phase (χ_M') and out-of-phase (χ_M") components of the ac susceptibility measured on powder at 2 K and 2000 Oe with the best fitted curves (red lines) for **6**.

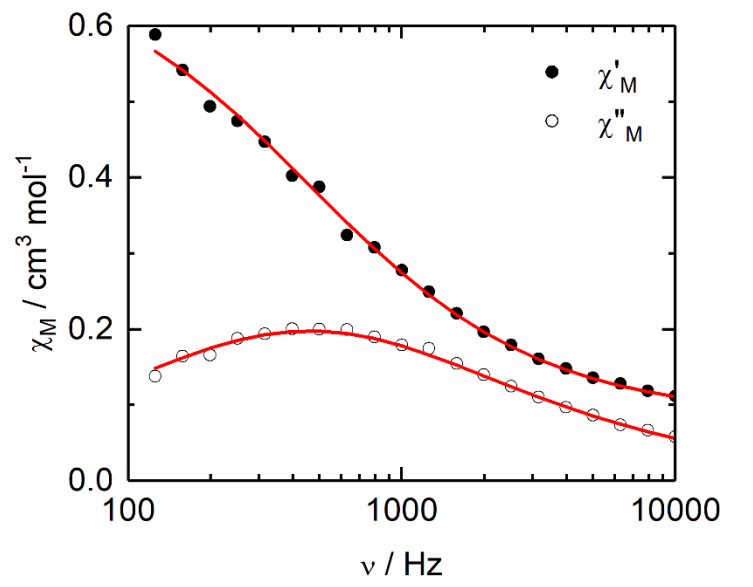

Figure S29. Frequency dependence of the in-phase (χ_M') and out-of-phase (χ_M") components of the ac susceptibility measured on powder at 2 K and 2200 Oe with the best fitted curves (red lines) for **7**.

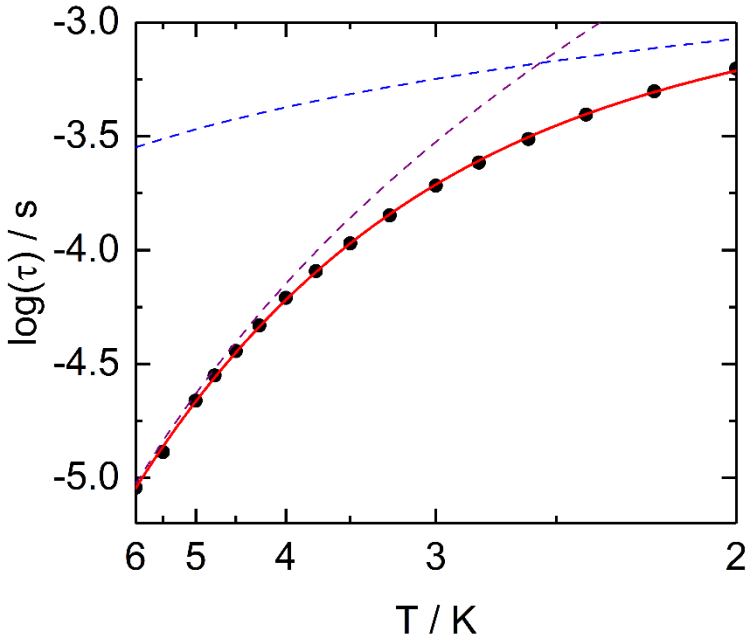

Figure S30. Temperature dependence of the relaxation time in a 1000 Oe applied magnetic field (full black disks) for **5** with the best-fitted curve (red line) and the two decomposed Raman (dashed purple line) and Direct (dashed blue line) relaxation processes in the temperature range of 2-6 K.

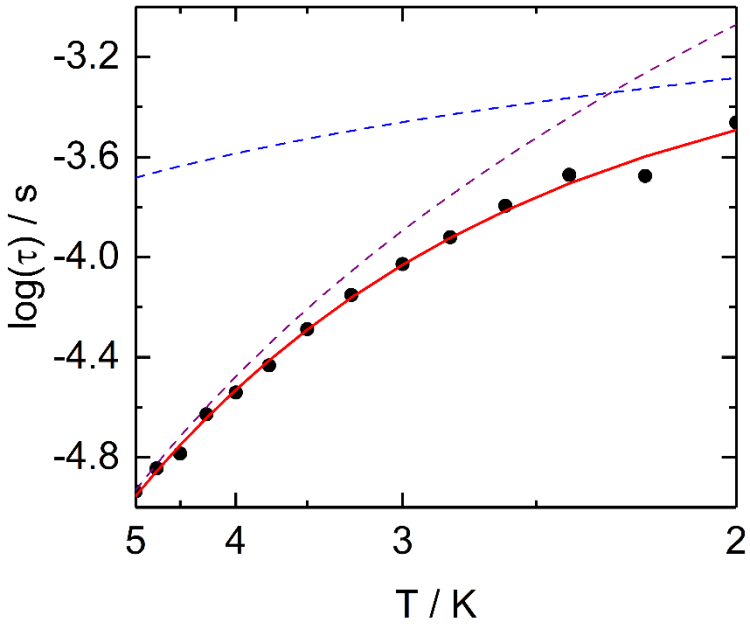

Figure S31. Temperature dependence of the relaxation time in a 2200 Oe applied magnetic field (full black disks) for **7** with the best-fitted curve (red line) and the two decomposed Raman (dashed purple line) and Direct (dashed blue line) relaxation processes in the temperature range of 2-5 K.

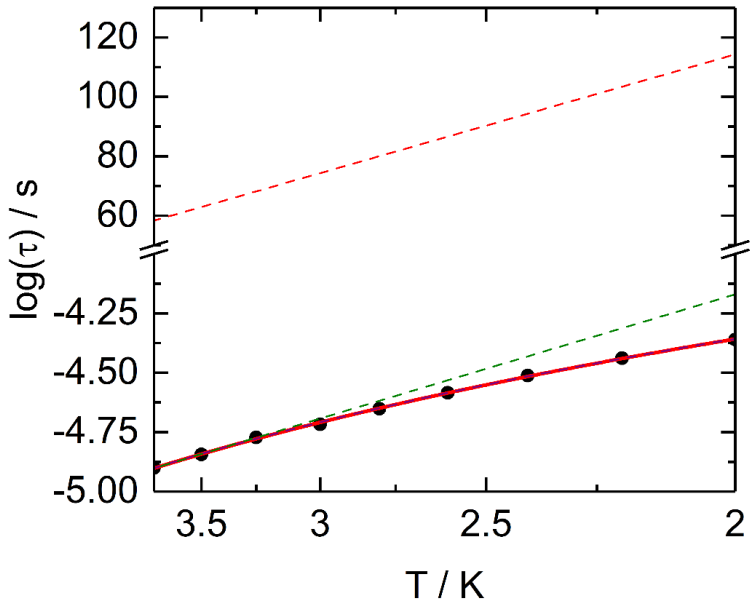

Figure S32. Temperature dependence of the relaxation time in a 1700 Oe applied magnetic field (full black disks) for **4** with the best-fitted curve (full red line) obtained with the combination of Raman (dashed purple line, B = 5741(119) s^{-1} $K^{-1.99}$ and n = 1.99(2)) and Orbach (dashed red line, Δ = 552 K and $\tau_0 = 2.8\times10^{-6}$ s) relaxation processes in the temperature range of 2-3.75 K. The dashed green line represents the Orbach relaxation process extracted from the high temperature data (Δ = 7.2(2) K and $\tau_0 = 1.8(1)\times10^{-6}$ s).

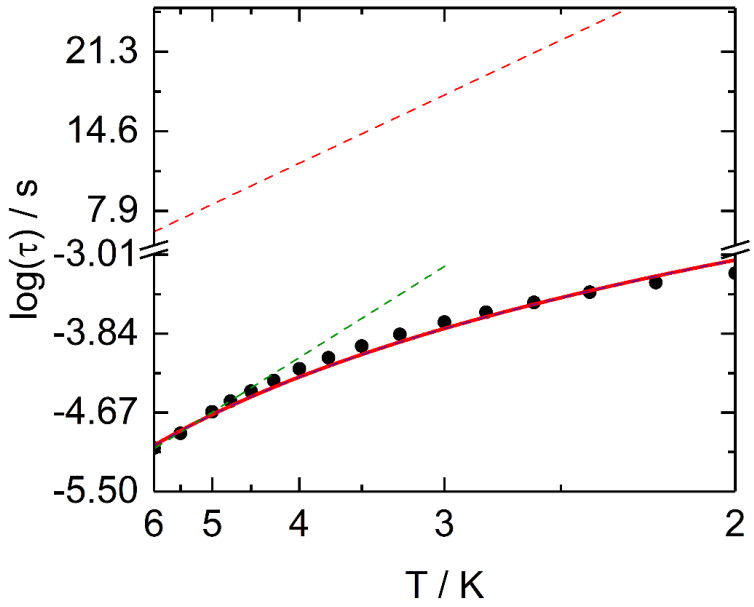

Figure S33. Temperature dependence of the relaxation time in a 1000 Oe applied magnetic field (full black disks) for **5** with the best-fitted curve (full red line) obtained with the combination of Raman (dashed purple line, B = 68(14) s^{-1} $K^{-4.1}$ and n = 4.1(2)) and Orbach (dashed blue line, Δ = 159 K and $\tau_0 = 0.4\times10^{-6}$ s) relaxation processes in the temperature range of 2-6 K. The dashed green line represents the Orbach relaxation process extracted from the high temperature data (Δ = 27(1) K and $\tau_0 = 1.1(3)\times10^{-7}$ s).

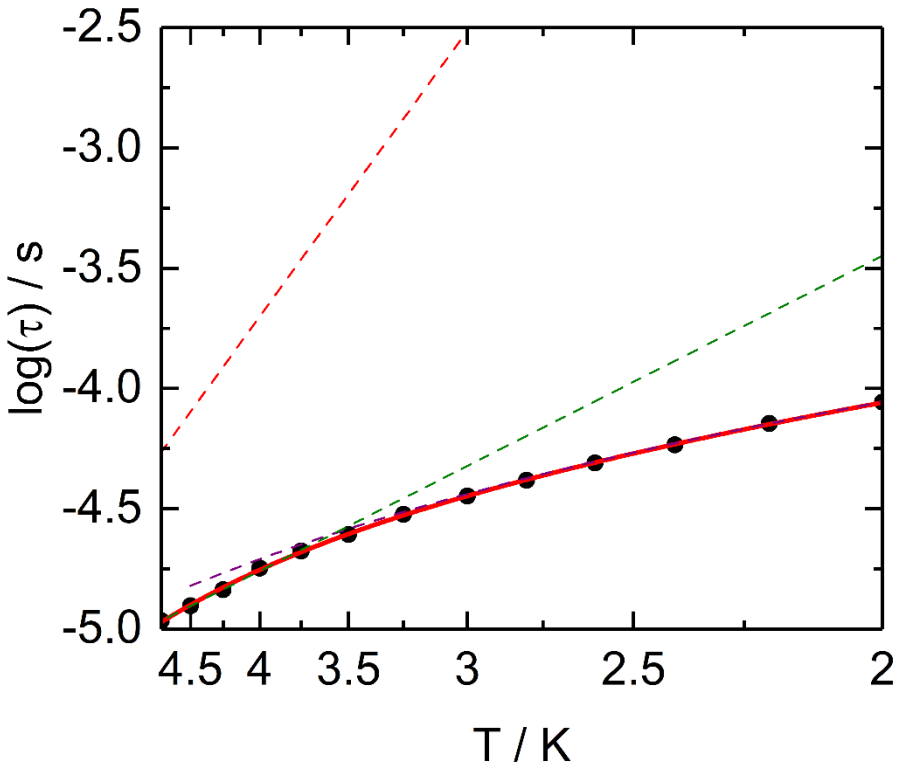

Figure S34. Temperature dependence of the relaxation time in a 2000 Oe applied magnetic field (full black disks) for **6** with the best-fitted curve (full red line) obtained with the combination of Raman (dashed purple line, B = 2530(102) s^{-1} $K^{-2.18}$ and n = 2.18(4)) and Orbach (dashed blue line, Δ = 32(5) K and $\tau_0 = 0.5\times10^{-8}$ s) relaxation processes in the temperature range of 2-4.75 K. The dashed green line represents the Orbach relaxation process extracted from the high temperature data (Δ = 12.1(1) K and $\tau_0 = 8(2)\times10^{-7}$ s).

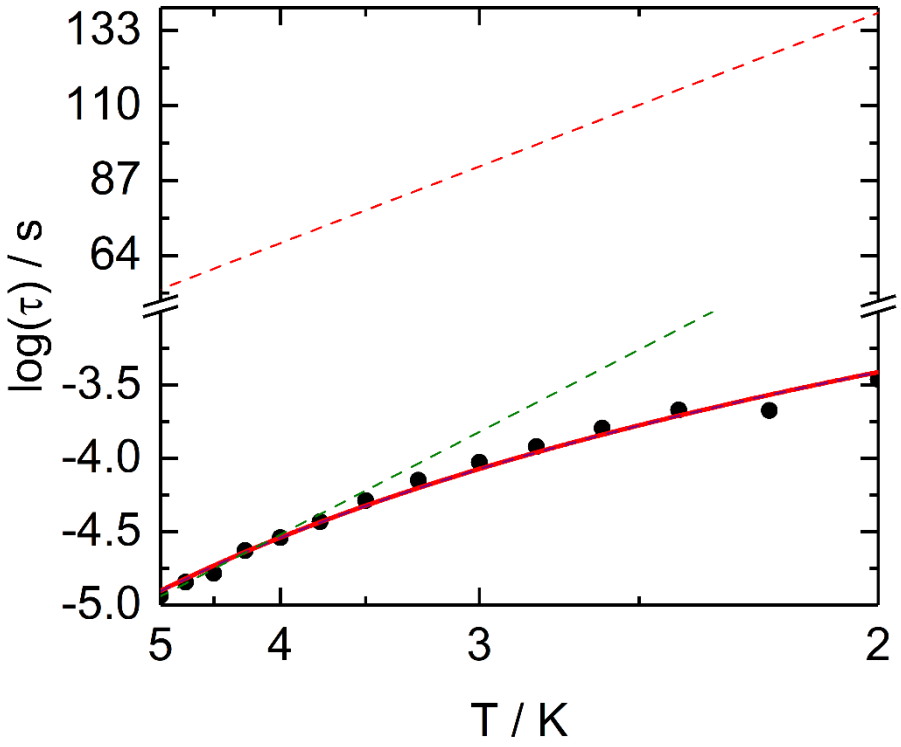

Figure S35. Temperature dependence of the relaxation time in a 2200 Oe applied magnetic field (full black disks) for **7** with the best-fitted curve (full red line) obtained with the combination of Raman (dashed purple line, B = 193(28) s^{-1} $K^{-3.7}$ and n = 3.7(1)) and Orbach (dashed blue line, Δ = 651 K and $\tau_0 = 1.2\times10^{-3}$ s) relaxation processes in the temperature range of 2-5 K. The dashed green line represents the Orbach relaxation process extracted from the high temperature data (Δ = 19.3(2) K and $\tau_0 = 2(1)\times10^{-7}$ s).

Table S1. X-ray crystallographic data for the complexes **1**-**7**.

Compounds	$[Ni(\mathbf{L^1})_2](NO_3)_2$ (**1**)	$[Co(\mathbf{L^1})_2](NO_3)_2$ (**2**)	$[Co(\mathbf{L^1})_2](BF_4)_2$ (**3**)	$[CoCl_2(\mathbf{L^1})](DMF)_2$ (**4**)
Formula	$C_{66}H_{52}N_{10}NiO_6S_{16}$	$C_{66}H_{52}N_{10}CoO_6S_{16}$	$C_{66}H_{52}N_{10}CoB_2F_8S_{16}$	$C_{39}H_{40}N_6CoCl_2O_2S_8$
M / g.mol^{-1}	1652.84	1653.06	1702.66	1011.08
Crystal system	Triclinic	Triclinic	Triclinic	Monoclinic
Space group	P-1 (N°2)	P-1 (N°2)	P-1 (N°2)	C2/c (N°15)
Cell parameters	a = 8.7378(12) Å	a = 8.7831(9) Å	a = 8.7286(11) Å	a = 38.288(4) Å
	b = 20.900(3) Å	b = 20.967(2) Å	b = 21.797(3) Å	b = 17.1339(15) Å
	c = 21.600(3) Å	c = 21.694(2) Å	c = 21.902(3) Å	c = 14.1680(11) Å
	α = 86.072(5)°	α = 78.851(4)°	α = 110.606(4)°	β = 90.527(3)°
	β = 82.765(5)°	β = 85.845(4)°	β = 91.881(4)°	
	γ = 82.765(5)°	γ = 82.362(4)°	γ = 100.558(5)°	
Volume / Å^3	3836.7(9)	3880.4(7)	3812.9(8)	9294.2(14)
Cell formula units	2	2	2	8
T / K	150 (2)	150(2)	150(2)	150(2)
Diffraction reflection	$4.65 \leq 2\theta \leq 55.31$	$4.64 \leq 2\theta \leq 51.36$	$4.56 \leq 2\theta \leq 55.08$	$4.26 \leq 2\theta \leq 55.10$
ρ_{calc}, g.cm^{-3}	1.431	1.415	1.483	1.445
μ, mm^{-1}	0.744	0.706	0.729	0.885
Number of reflections	81654	56940	73505	67662
Independent reflections	16907	14699	17112	10655
$Fo^2 > 2\sigma(Fo)^2$	7346	11129	9423	8050
Number of variables	892	895	878	536
R_{int}, R_1, ωR_2	0.2225, 0.1353, 0.2957	0.0763, 0.1205, 0.3094	0.1852, 0.1758, 0.3207	0.0351, 0.0598, 0.1672

Compounds	$[CoBr_2(\mathbf{L^1})]\cdot(DMF)$ (**5**)	$[CoCl_2(\mathbf{L^2})]\cdot(DMF)\cdot 0.5(Et_2O)$ (**6**)	$[CoBr_2(\mathbf{L^2})]\cdot(DMF)$ (**7**)
Formula	$C_{36}H_{33}N_5CoBr_2OS_8$	$C_{42}H_{46}N_5CoCl_2O_{1.5}S_8$	$C_{40}H_{41}N_5CoBr_2OS_8$
M / g.mol^{-1}	1026.90	1031.15	1083.01
Crystal system	Monoclinic	Monoclinic	Monoclinic
Space group	C2/c (N°15)	C2/c (N°15)	$P2_1/n$ (N°14)
Cell parameters	a = 18.4160(6) Å	a = 39.226(6) Å	a = 17.886(3) Å
	b = 13.2904(5) Å	b = 17.274(2) Å	b = 13.417(3) Å
	c = 34.1258(13) Å	c = 14.1155(18) Å	c = 37.960(8) Å
	β = 98.251(4)°	β = 90.769(5)°	β = 91.971(7)°
Volume / Å^3	8310.8(5)	9564(2)	9104(3)
Cell formula units	8	8	8
T / K	150 (2)	150(2)	150(2)
Diffraction reflection	$4.36 \leq 2\theta \leq 55.07$	$4.72 \leq 2\theta \leq 55.07$	$4.32 \leq 2\theta \leq 55.14$
ρ_{calc}, g.cm^{-3}	1.641	1.432	1.580
μ, mm^{-1}	2.775	0.860	2.538
Number of reflections	27011	66125	68821
Independent reflections	9175	10962	20057
$Fo^2 > 2\sigma(Fo)^2$	6314	8357	13144
Number of variables	482	536	1035
R_{int}, R_1, wR_2	0.0688, 0.0839, 0.1583	0.1081, 0.0853, 0.1678	0.0832, 0.0797, 0.1622

Table S2. Oxidation potentials of the ligands $\mathbf{L^1}$ and $\mathbf{L^2}$ (V *vs* SCE, nBu_4NPF_6, 0.1 M in CH_2Cl_2 at 100 mV.s^{-1}), and complexes **1**-**7** (V *vs* SCE, nBu_4NPF_6, 0.1 M in DMF at 100 mV.s^{-1}).

	$E^1_{1/2}$ / V		$E^2_{1/2}$ / V		$E^3_{1/2}$ / V		$E^3_{1/2}$ / V	
	$^{ox}E^1_{1/2}$	$^{red}E^1_{1/2}$	$^{ox}E^2_{1/2}$	$^{red}E^2_{1/2}$	$^{ox}E^3_{1/2}$	$^{red}E^3_{1/2}$	$^{ox}E^4_{1/2}$	$^{red}E^4_{1/2}$
$\mathbf{L^1}$	/	/	0.64	0.46	1.00	0.83	/	/
$\mathbf{L^2}$	/	/	0.61	0.44	0.97	0.79	/	/
1	/	/	0.78	0.60	0.95	0.78	/	/
2	0.34	0.23	0.76	0.62	0.92	0.79	/	/
3	0.33	0.25	0.72	0.64	0.88	0.77	/	/
4	0.34*	0.21*	0.75	0.62	0.90	0.77	1.11	0.96
5	0.32*	0.24*	0.74	0.63	0.94	0.78	0.74	/
6	0.33*	0.20*	0.73	0.63	0.84	0.75	1.14	0.98
7	0.36*	0.26*	0.76	0.63	0.92	0.78	0.76	/

Table S3. Best fitted parameters (χ_T, χ_S, τ and α) with the extended Debye model for compound **4** at 2 K in the magnetic field range 400-3000 Oe.

H / Oe	χ_S / cm^3 mol^{-1}	χ_T / cm^3 mol^{-1}	τ / s	α	R^2
400	0.59376	0.92328	2.10206E-5	0.10247	0.99989
600	0.36158	0.91393	2.51675E-5	0.11521	0.99968
800	0.21475	0.91084	2.98415E-5	0.14087	0.99989
1000	0.13664	0.89774	3.45849E-5	0.1453	0.99938
1200	0.09282	0.88273	3.87388E-5	0.14917	0.99948
1400	0.05014	0.86963	4.12138E-5	0.17198	0.9992
1600	0.03715	0.8404	4.34818E-5	0.16452	0.99968
1800	0.02208	0.81832	4.49015E-5	0.17346	0.99978
2000	0.00494	0.79603	4.52656E-5	0.18847	0.99908
2200	1.87E-15	0.77858	4.65123E-5	0.19843	0.9979
2400	2E-15	0.75127	4.69615E-5	0.20404	0.99752
2600	2E-15	0.71778	4.62383E-5	0.20034	0.99918
2800	2E-15	0.69309	4.57955E-5	0.20456	0.99894
3000	2E-15	0.6709	4.56209E-5	0.21833	0.99828

Table S4. Best fitted parameters (χ_T, χ_S, τ and α) with the extended Debye model for compound **5** at 2 K in the magnetic field range 200-3000 Oe.

H / Oe	χ_S / cm^3 mol^{-1}	χ_T / cm^3 mol^{-1}	τ / s	α	R^2
200	0.55687	0.83726	4.05124E-4	0.09916	0.99906
400	0.30301	0.84429	5.30448E-4	0.09112	0.99922
600	0.1796	0.85213	6.10263E-4	0.12159	0.99911
800	0.12046	0.85031	6.38594E-4	0.13059	0.99957
1000	0.08859	0.83894	6.40383E-4	0.13032	0.99975
1200	0.06946	0.81919	6.24638E-4	0.12682	0.99933
1400	0.05335	0.80653	6.24265E-4	0.14089	0.99942
1600	0.04555	0.79274	6.12396E-4	0.14063	0.99957
1800	0.03864	0.78951	6.14957E-4	0.15045	0.99911
2000	0.03162	0.76453	5.91846E-4	0.1587	0.99874
2200	0.0288	0.746	5.71886E-4	0.1577	0.99902
2400	0.02262	0.73002	5.60916E-4	0.17389	0.99923
2600	0.0176	0.70619	5.31254E-4	0.18405	0.99757
2800	0.01735	0.68886	5.00534E-4	0.18066	0.99764
3000	0.01033	0.66977	4.77394E-4	0.20297	0.99647

Table S5. Best fitted parameters (χ_T, χ_S, τ and α) with the extended Debye model for compound **6** at 2 K in the magnetic field range 400-3000 Oe.

H / Oe	χ_S / cm^3 mol^{-1}	χ_T / cm^3 mol^{-1}	τ / s	α	R^2
400	1.52857	2.23919	4.01496E-5	0.05004	0.99986
600	1.01412	2.22719	5.16846E-5	0.06854	0.99989
800	0.67469	2.21355	6.1916E-5	0.09304	0.9998
1000	0.4768	2.17808	7.06652E-5	0.10304	0.99979
1200	0.35636	2.13249	7.71283E-5	0.11037	0.99981
1400	0.27041	2.08964	8.25696E-5	0.12386	0.99971
1600	0.21498	2.03955	8.65083E-5	0.13225	0.99976
1800	0.16323	1.99079	8.91548E-5	0.14861	0.99965
2000	0.13193	1.92836	9.02322E-5	0.15592	0.99964
2200	0.10054	1.86858	9.00516E-5	0.17068	0.99983
2400	0.08386	1.79274	8.87834E-5	0.17403	0.99918
2600	0.04607	1.76186	8.85354E-5	0.20442	0.99885
2800	0.03274	1.69894	8.71746E-5	0.21271	0.99949
3000	0.02337	1.60643	8.24731E-5	0.21265	0.99934

Table S6. Best fitted parameters (χ_T, χ_S, τ and α) with the extended Debye model for compound **7** at 2 K in the magnetic field range 400-3000 Oe.

H / Oe	χ_S / cm^3 mol^{-1}	χ_T / cm^3 mol^{-1}	τ / s	α	R^2
400	0.46255	0.74743	1.353E-4	0.24196	0.99983
600	0.34068	0.7471	1.67832E-4	0.22436	0.99919
800	0.24368	0.76007	1.99635E-4	0.27192	0.99938
1000	0.20005	0.74113	2.08714E-4	0.22834	0.99949
1200	0.16943	0.71699	2.19656E-4	0.20345	0.99802
1400	0.13869	0.72387	2.38329E-4	0.22329	0.99725
1600	0.12948	0.6563	2.10505E-4	0.15573	0.99605
1800	0.11186	0.66082	2.28598E-4	0.18853	0.99837
2000	0.10307	0.67048	2.4712E-4	0.18242	0.9953
2200	0.08615	0.66703	2.52652E-4	0.21165	0.99832
2400	0.06504	0.68222	2.78554E-4	0.27614	0.99754
2600	0.08111	0.62277	2.38005E-4	0.17983	0.98896
2800	0.07397	0.61479	2.38092E-4	0.18765	0.99377
3000	0.05593	0.6362	2.54292E-4	0.25971	0.99495

Table S7. Best fitted parameters (χ_T, χ_S, τ and α) with the extended Debye model for compound **4** at 1700 Oe in the temperature range 2-3.75 K.

T / K	χ_T / cm^3 mol^{-1}	χ_S / cm^3 mol^{-1}	α	τ / s	R^2
2	0.82169	0.02181	0.17855	4.35848E-5	0.99982
2.2	0.77294	0.02419	0.16409	3.64245E-5	0.99986
2.4	0.72349	0.02896	0.14876	3.0728E-5	0.99988
2.6	0.68255	0.02708	0.14635	2.60169E-5	0.99988
2.8	0.64149	0.02923	0.13722	2.22836E-5	0.99975
3	0.6053	0.02827	0.1332	1.91855E-5	0.99987
3.25	0.56449	0.04556	0.11205	1.6896E-5	0.99934
3.5	0.52694	0.04576	0.10383	1.43176E-5	0.99982
3.75	0.49673	0.05327	0.09721	1.25699E-5	0.99984

Table S8. Best fitted parameters (χ_T, χ_S, τ and α) with the extended Debye model for compound **5** at 1000 Oe in the temperature range 2-6 K.

T / K	χ_T / cm^3 mol^{-1}	χ_S / cm^3 mol^{-1}	α	τ / s	R^2
2	0.82428	0.09099	0.11639	6.25958E-4	0.99952
2.2	0.76431	0.08393	0.1166	4.97984E-4	0.9981
2.4	0.70637	0.07702	0.11548	3.93674E-4	0.99859
2.6	0.64725	0.07319	0.10295	3.0718E-4	0.99843
2.8	0.60186	0.07029	0.09116	2.42248E-4	0.99841
3	0.56341	0.06785	0.0816	1.91633E-4	0.99904
3.25	0.51875	0.0642	0.07112	1.42099E-4	0.99718
3.5	0.48645	0.0609	0.06689	1.07076E-4	0.99764
3.75	0.45542	0.05908	0.0574	8.08123E-5	0.9986
4	0.43071	0.05767	0.05111	6.16303E-5	0.99647
4.25	0.40495	0.05406	0.04656	4.66172E-5	0.99639
4.5	0.37956	0.05681	0.02043	3.59818E-5	0.99623
4.75	0.36063	0.05769	0.00928	2.81599E-5	0.99864
5	0.347	0.05243	0.02291	2.1816E-5	0.99861
5.25	0.31848	0.0416	0.03321	1.29625E-5	0.99751
5.5	0.29005	0.05717	0	9.03927E-6	0.9986
6	0.82428	0.09099	0.11639	6.25958E-4	0.99952

Table S9. Best fitted parameters (χ_T, χ_S, τ and α) with the extended Debye model for compound **6** at 1000 Oe in the temperature range 2-4.75 K.

T / K	χ_T / cm^3 mol^{-1}	χ_S / cm^3 mol^{-1}	α	τ / s	R^2
2	0.8794	0.04966	0.16718	8.76081E-5	0.99948
2.2	0.83515	0.05265	0.15256	7.14004E-5	0.99913
2.4	0.7758	0.06239	0.11988	5.82511E-5	0.99929
2.6	0.744	0.05233	0.13016	4.89531E-5	0.99884
2.8	0.69666	0.06367	0.09969	4.15408E-5	0.99947
3	0.65841	0.06826	0.07922	3.5717E-5	0.99921
3.25	0.61785	0.07125	0.06633	2.99413E-5	0.99887
3.5	0.58534	0.06367	0.07266	2.46795E-5	0.99921
3.75	0.55175	0.07053	0.05329	2.10836E-5	0.9996
4	0.51908	0.0766	0.03248	1.78936E-5	0.99943
4.25	0.49352	0.06668	0.04163	1.45625E-5	0.99971
4.5	0.46547	0.07313	0.01712	1.24724E-5	0.99971
4.75	0.44369	0.08091	0.00378	1.07985E-5	0.99963

Table S10. Best fitted parameters (χ_T, χ_S, τ and α) with the extended Debye model for compound **7** at 2200 Oe in the temperature range 2-5 K.

T / K	χ_T / cm^3 mol^{-1}	χ_S / cm^3 mol^{-1}	α	τ / s	R^2
2	0.70078	0.07792	0.27972	3.45105E-4	0.99729
2.2	0.58429	0.08148	0.2053	2.11213E-4	0.98553
2.4	0.61936	0.06411	0.28072	2.13102E-4	0.99482
2.6	0.56473	0.07174	0.22519	1.60357E-4	0.99681
2.8	0.52183	0.06687	0.20499	1.20049E-4	0.99742
3	0.49335	0.06333	0.19716	9.38225E-5	0.99658
3.25	0.47437	0.04768	0.22907	7.06052E-5	0.99702
3.5	0.43681	0.06175	0.16422	5.15148E-5	0.99785
3.75	0.41243	0.05205	0.16869	3.69499E-5	0.9953
4	0.38606	0.05992	0.12713	2.87779E-5	0.99577
4.25	0.35968	0.0811	0.0553	2.3515E-5	0.9963
4.5	0.35005	0.05547	0.11247	1.64184E-5	0.99761
4.75	0.32994	0.07629	0.05043	1.43169E-5	0.99663
5	0.32136	0.08191	0.06683	1.15735E-5	0.99338